

Core collapse supernovae. Magnetorotational explosion.

G.S.Bisnovatyi-Kogan^{1,2}, S.G.Moiseenko¹ and N.V.Ardeljan³

¹*IKI RAS, Profsoyuznaya 84/32, Moscow 117997, Russia*

²*JINR, Dubna, Russia*

³*Department of Computational Mathematics and Cybernetics, Moscow State University,*

Vorobjevy Gory, Moscow B-234, Russia

email: gkogan@iki.rssi.ru

Abstract

Core-collapse supernovae are connected with formation of neutron stars. Part of the gravitation energy is transformed into the energy of the explosion, observed in SN II, SN Ib,c type supernovae. The mechanism of transformation is not simple, because the overwhelming majority of the energy is going into weakly interacting neutrino. The attempts to use this energy for the explosion were not successful during about 40 years of investigation. We consider the explosion mechanism in which the source of energy is the rotation, and magnetic field serves for the transformation of the rotation energy into the energy of explosion. 2-D MHD simulations of this mechanism were performed. After the collapse the core consists of a rapidly rotating proto-neutron star with a differentially rotating envelope. The toroidal part of the magnetic energy generated by the differential rotation grows as quadratic function with time at the initial stage of the evolution of the magnetic field. The linear growth of the toroidal magnetic field is terminated by the development of magnetohydrodynamic instability, when the twisted toroidal component strongly exceeds the poloidal field, leading to a drastic acceleration in the growth of magnetic energy. At the moment when the magnetic pressure becomes comparable to the gas pressure at the periphery of the proto-neutron star the MHD compression wave appears and goes through the envelope of the collapsed core. It transforms into the fast MHD shock and produces a supernova explosion. Our simulations give the energy of the explosion $0.6 \cdot 10^{51}$ ergs. The amount of the mass ejected by the explosion is $\sim 0.14M_{\odot}$. The implicit numerical method, based on the Lagrangian triangular grid of variable structure, was used for the simulations.

Keywords: supernovae, collapse, magnetohydrodynamics.

1 Introduction

Content.

1. Presupernovae.
2. Magnetorotational mechanism of explosion: 1-D calculations.
3. 2-D MHD: Numerical method.
4. Core collapse and formation of rapidly rotating neutron star.
5. Magnetorotational supernova explosion.
6. Development of magnetorotational instability.
7. Jet formation in magnetorotational SN explosion.
8. Mirror symmetry breaking: Rapidly moving pulsars. One-side jets.

Supernova is one of the most powerful explosions in the Universe, producing the energy (radiation and kinetic) about 10^{51} erg. The explosion happens at the end of the evolution of massive stars, with initial mass more than ~ 8 Solar masses. Hertzsprung-Russell diagram of the zero age main sequence, and several evolutionary tracks are represented in left side of Fig.1 from [20]. Tracks in HR diagram of a representative selection of stars from the main sequence till the end of the evolution are given in the right side of Fig.1 from [16].

The explosion mechanisms are:

1. Thermonuclear explosion of C-O degenerate core (SN Ia)
2. Core collapse and formation of a neutron star, with a gravitational energy release $\sim 6 \cdot 10^{53}$ erg, carried away by neutrino (SN II, SN Ib,c).

The transformation of the neutrino energy into kinetic one is very problematic, and was not obtained firmly. Magnetorotational explosion (MRE), in the core collapse SN, is based on the transformation of the rotational energy of the neutron star into the explosion energy by means of the magnetic field.

Most of supernova explosions and ejections are not spherically symmetrical. A lot of stars are rotating and have magnetic fields. Often we can see one-side ejections. One of the main difficulties for core collapse supernova explosions is, how to transform any kind of energy of the star into the explosion energy. The magnetorotational mechanism suggested in [9], transforms the rotational energy of the star into the explosion energy with a high efficiency of about 10%. It is acting in presence of the differential rotation when the rotational energy can be transformed to the explosion energy by the magnetic field action.

2 1-D calculations

1-D calculations of the magnetorotational explosion (MRE) have been performed first in [12]. The important parameter of the problem is the ratio of the magnetic and gravitational energies at the initial moment, when differential rotation starts to twist and to amplify the toroidal component, $\alpha = \frac{E_{mag0}}{E_{grav0}}$. In [12] rather large values of $\alpha = 0.1$ and 0.01 had been considered, see Figs.2,3.

1-D calculations of MRE for lower magnetic fields, at $\alpha = 10^{-2}$, 10^{-4} , 10^{-8} , had been done in [5], see Fig.4. Angular velocity distribution at different time moments. is represented in Fig.5 form [12]. Variations of different types of kinetic energy during MRE are given in Fig.6 from [12].

The main results of 1-D calculations are the following. Magneto-rotational explosion (MRE) has an efficiency about 10% of rotational energy. For the neutron star with mass $\approx 1.2M_{\odot}$ the ejected mass is about $0.1M_{\odot}$, the explosion energy is about 10^{51} erg. Ejected mass and explosion energy depend weakly on the parameter α , explosion time strongly depends on α , Explosion time $t_{expl} \sim 1/\sqrt{\alpha}$ [5]. Small α is difficult for numerical calculations with EXPLICIT numerical schemes because of the Courant restriction on the time step for a stiff set of equations: small α determines a stiffness. In 2-D numerical an IMPLICIT numerical schemes should be used.

3 The difference scheme for 2-D calculations

First 2-D calculations, showing jets in the collapse of rotating magnetized star had been performed in [18]. Very large magnetic field was taken, so twisting of magnetic field lines, expected in a realistic situation, was not important for the explosion, see Figs.7,8.

The difference scheme used in the present calculations is described in [7], [6]. The scheme is based on the method of basic operators - grid analogs of the main differential operators:

GRAD(scalar) (differential) GRAD(scalar) (grid analog)
 DIV(vector) (differential) DIV(vector) (grid analog)
 CURL(vector) (differential) CURL(vector) (grid analog)
 GRAD(vector) (differential) GRAD(vector) (grid analog)
 DIV(tensor) (differential) DIV(tensor) (grid analog)

The scheme is implicit. It was developed, and its stability and convergence was investigated by the group of N.V.Ardeljan in Moscow State University. The scheme is fully conservative, providing conservation of the mass, momentum and total energy, and giving correct calculation of the transitions between different types of energies. Matrices for the transformation are symmetrical. The difference scheme is Lagrangian, with triangular grid, and possibility of grid reconstruction, see Fig.9. The angular momentum conserves automatically in this scheme.

The astrophysical application of this scheme was started by calculations of a collapse of a non-magnetized rotating protostellar cloud, important in the problem of star formation [1]. Rigidly rotating uniform gas sphere was considered for initial conditions. The cloud, as a rigidly rotating uniform gas sphere, was taken with the following initial parameters:

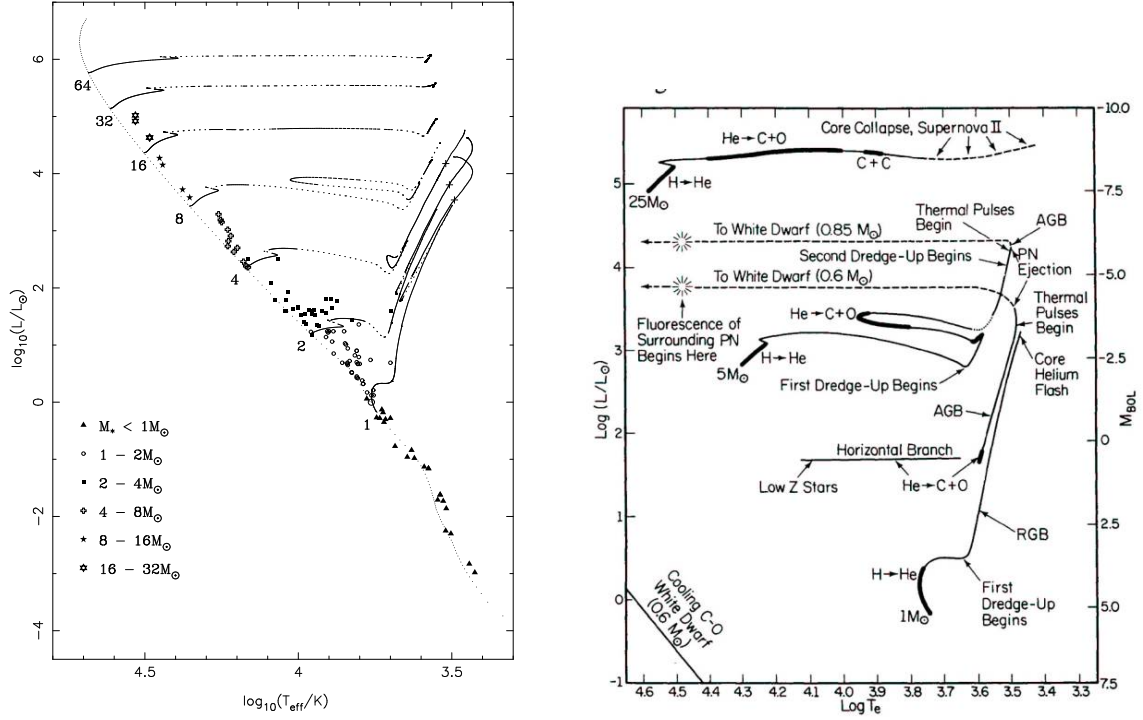


Figure 1: **Left.** Hertzsprung–Russell diagram of the ZAMS and several evolutionary tracks. The masses of the models are indicated at the starts of the tracks, in solar units. The solid portions of the tracks indicate where evolution is on a relatively slow nuclear time-scale, the dotted parts show evolution on a thermal time-scale, and the dashed parts show an intermediate time-scale. The different symbols indicate the positions of binary components with well-determined masses, radii and luminosities. The position of the Sun is indicated by a solar symbol \odot . The crosses (+) show the position on the giant branches of the 1-, 2- and 4- M_{\odot} models where the binding energy of the envelope becomes positive, from [20].

Right. Coarse evolutionary tracks for stars with $M_i = 1, 5, 25 M_{\odot}$. Heavy portions represent principal burning phases in the core. For $M_i < 2.3 M_{\odot}$, CHF (core helium flash) occurs after which quiescent ${}^4\text{He}$ burning begins. After ${}^4\text{He}$ has been exhausted in the core, the star arrives on the AGB (asymptotic giant branch). When the core with no helium in it reaches the mass $\sim 0.53 M_{\odot}$, TF (thermal flashes in ${}^4\text{He}$ shell) start. An AGB star loses mass, and this process terminates with a rapid ejection of the residual hydrogen envelope in the form of PN (planetary nebula). CO core with $M_f \approx 0.6 M_{\odot}$ transforms into white dwarf. More massive AGB and post-AGB stars with $M_i \leq 9 M_{\odot}$ evolve in a similar way, M_f increases with increasing M_i and equals $1.08 M_{\odot}$ at $M_i = 8.8 M_{\odot}$. The symbol \circ indicates the onset of planetary nebula luminescence, when T_{ef} of the star reaches $3 \cdot 10^4$ K and the gas ionization in PN begins, from [16].

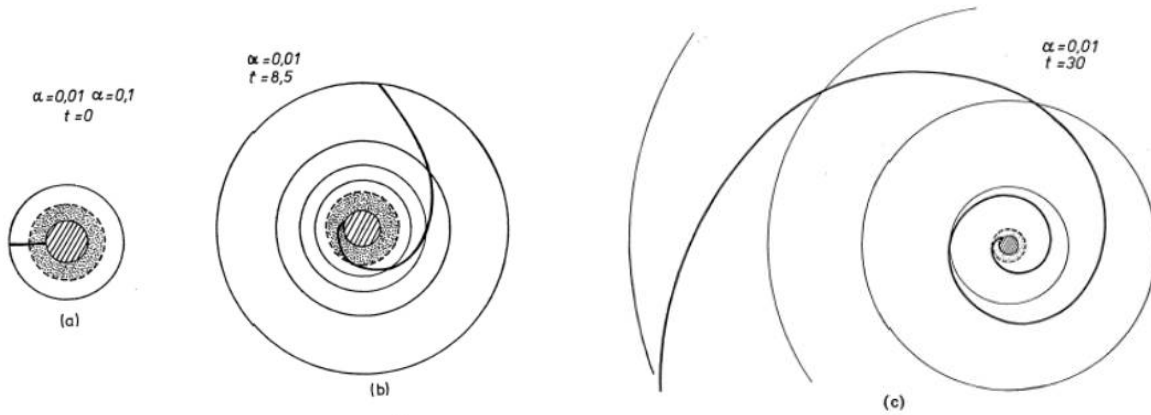


Figure 2: The configuration of the magnetic field line in the subsequent moments of time for $\alpha = 0.01$. The dashed region is the central incompressible core of the neutron star; the pointed region is a contracting part of the envelope. In the right figure (c) the scale is diminished to a half in comparison with (a) and (b), from [12].

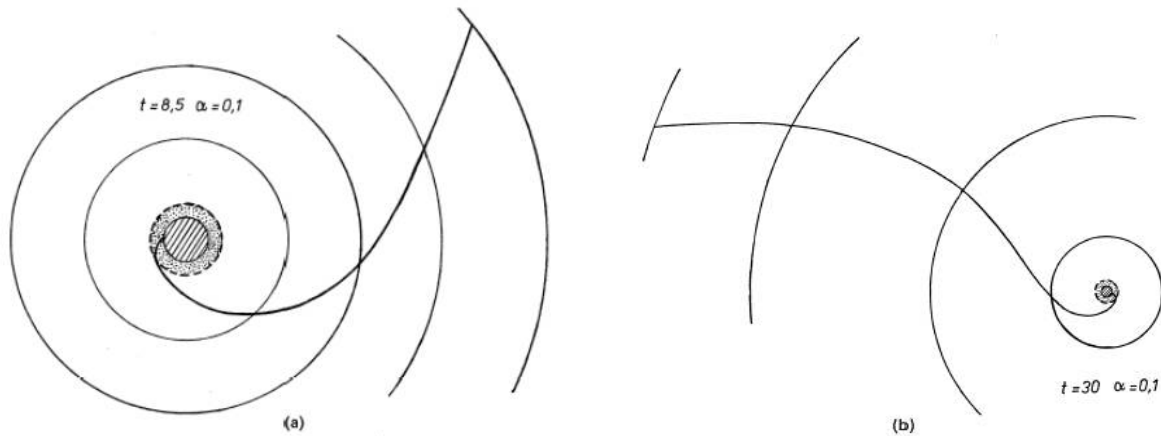


Figure 3: The same picture as in Fig.2, but for $\alpha = 0.1$. The initial picture coincides with Fig.2. In the figure (b) the scale is diminished four times, from [12].

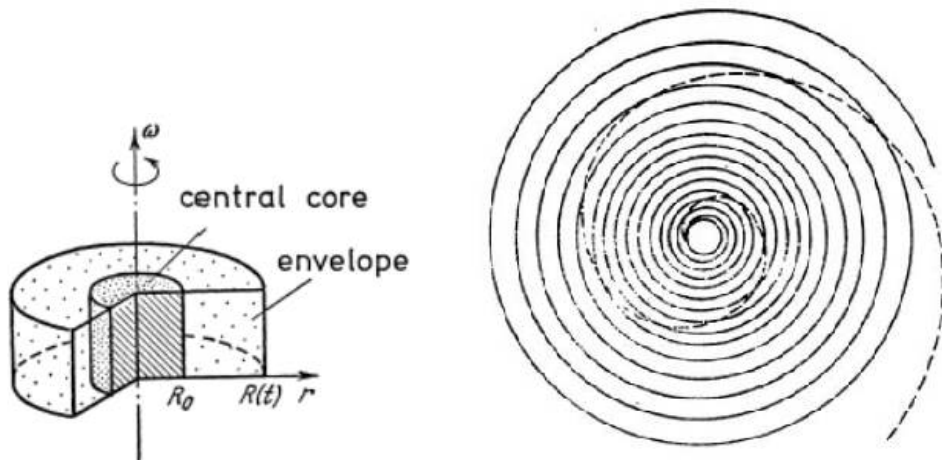


Figure 4: **left** A schematic picture of the initial state for the unit length of the cylinder, from [12]. **right** Shape of the field lines in the region near the core at the time $t = 7/\sqrt{\alpha}$, for $\alpha = 0.01$ (dashed line), and $\alpha = 10^{-4}$ (solid line), from [5].

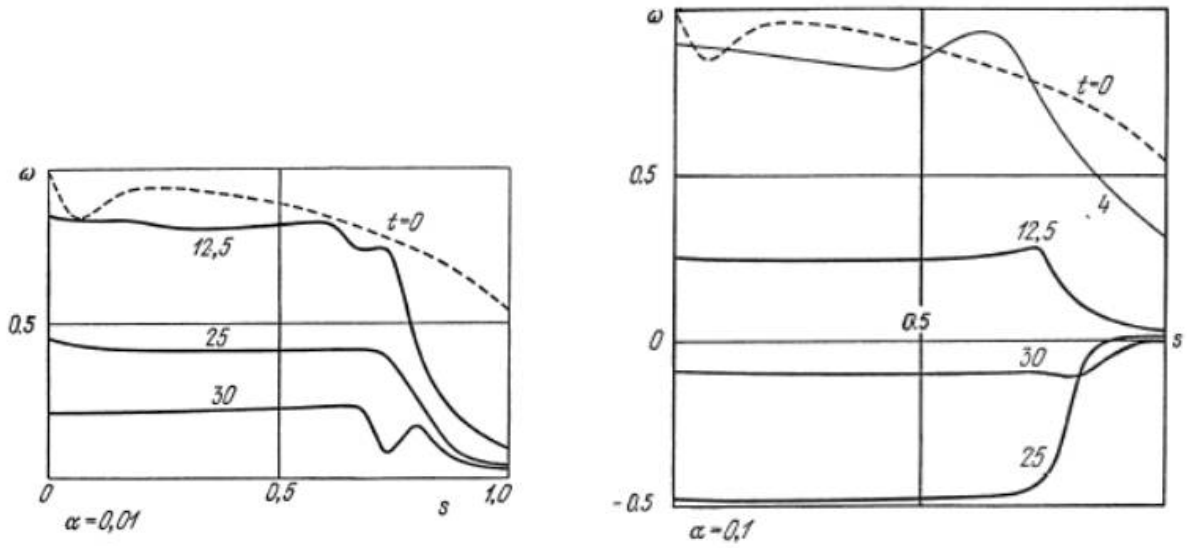


Figure 5: The dependence of the angular velocity ω on the mass coordinate s at later time for two values of the parameter α . The division of the envelope in two parts is seen: the uniformly rotating central part, and the ejected outer part, in which the rotation became slower. The change of the direction of rotation is seen on the right figure, from [12].

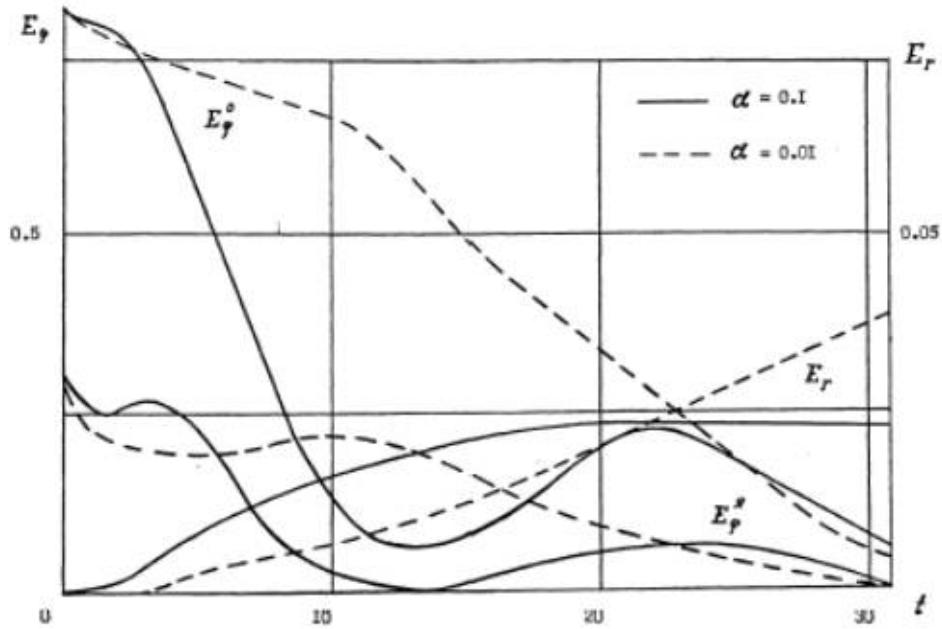


Figure 6: The dependence of the kinetic energy on time for two values of α : the rotational energy of the core E_ϕ , envelope E_ϕ^0 , the radial energy of the envelope E_r , from [12].

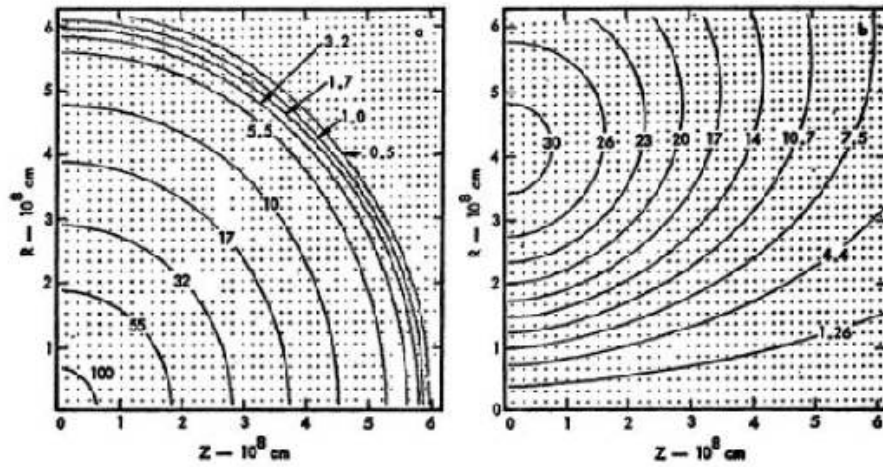


Figure 7: Isodensity contours in units of 10^6 g/cm^3 (a), and magnetic-flux contours parallel to Z-axis in units of $10^{22} \text{ Gs/cm}^{-2}$ (b), at 0.72 sec, from [18].

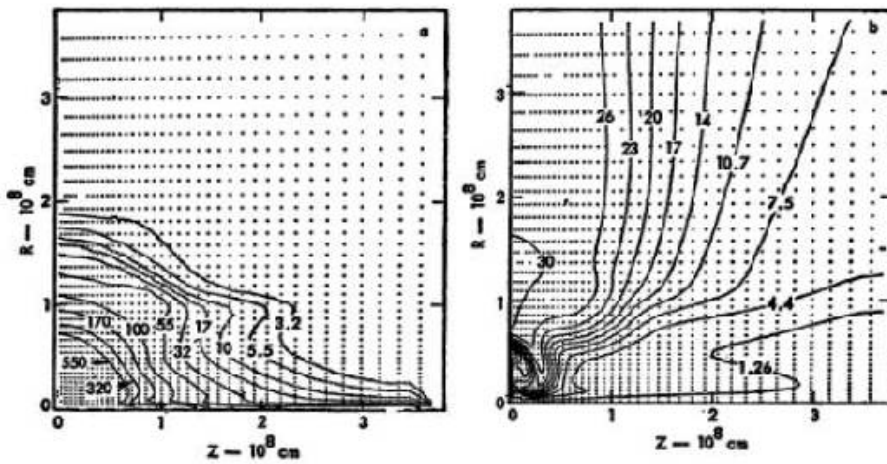


Figure 8: Isodensity contours in units of 10^6 g/cm^3 (a), and magnetic-flux contours parallel to Z-axis in units of $10^{22} \text{ Gs/cm}^{-2}$ (b), at 2.67 sec, from [18].

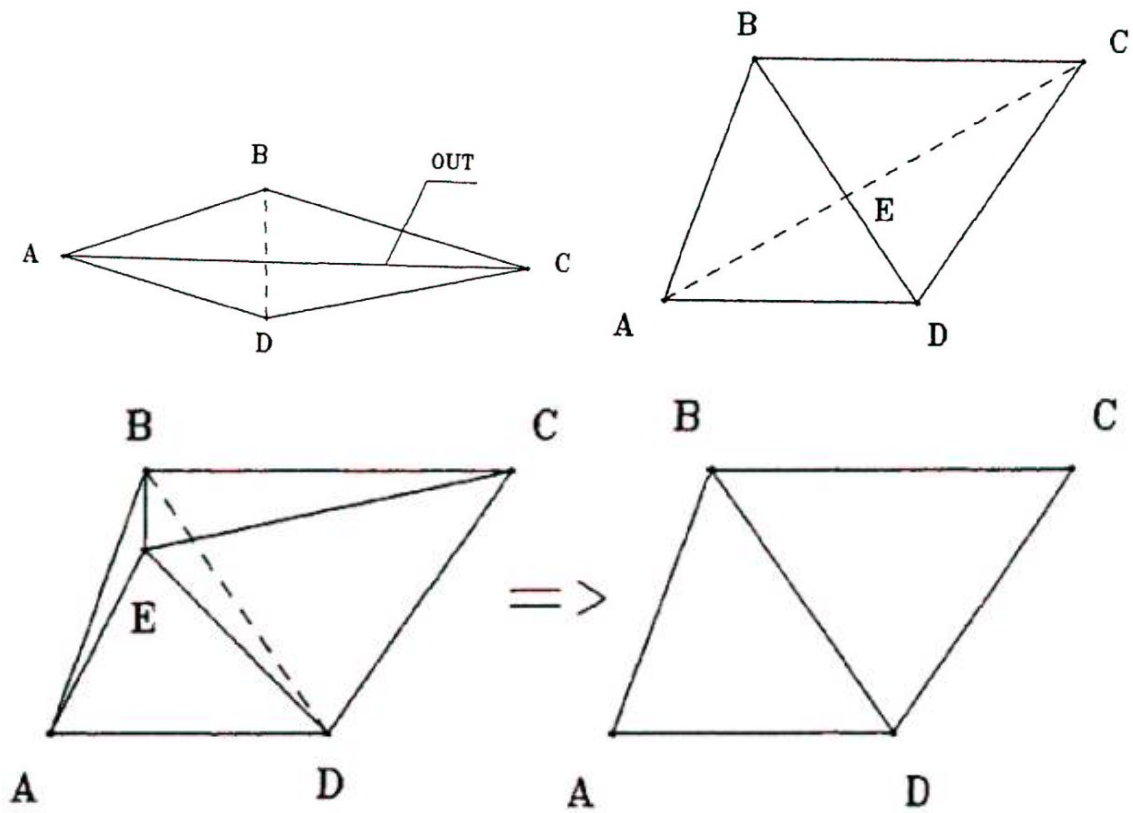


Figure 9: Elementary reconstructions: (Left up) BD connection is introduced instead of AC connection. The total number of knots and cells in the grid is not changed. (Right up) Adding a knot at the middle of the connection: the knot E is added to the existing knots ABCD in the middle of BD connection, 2 connections AE and EC appear, and the total number of cells is increased by 2 cells. (Down) Removing a knot: the knot E is removed from the grid, and the total number of cells is decreased by 2 cells, from [1]

$$\rho = 1.492 \cdot 10^{-17} g/cm^3, \quad p = 1.548 \cdot 10^{-10} dyn/cm^2, \quad r = 3.81 \cdot 10^{16} cm, \quad (1)$$

$$\omega = 2.008 \cdot 10^{-12} rad/sec, \quad M = 1.73 M_{\odot} = 3.457 \cdot 10^{33} g, \quad \gamma = 5/3, \quad u^r = u^z = 0.$$

On the outer boundary the pressure was taken to be equal to a small constant ($p = 0.87 \cdot 10^{-13}$ dyn/cm²). At the outer boundary of the cloud, the gravitational potential Φ is defined by the integral Poisson formula, using the expression for the volume potential. The results of calculations, showing formation of the bounce shock, and subsequent outburst are represented in Fig.10 from [1].

4 Presupernova Core Collapse

Collapse and formation of a rapidly and differentially rotating neutron star had been calculated in [2] in non-magnetized approximation. Equations of state takes into account degeneracy of electrons and neutrons, relativity for the electrons, nuclear transitions and nuclear interactions. Temperature effects were taken into account approximately by the addition of the pressure of radiation and of an ideal gas. Neutrino losses and iron dissociation were taken into account in the energy equations. A cool white dwarf was considered at the stability limit with a mass equal to the Chandrasekhar limit. To obtain the collapse we increase the density at each point by 20% and switch on a uniform rotation.

The hydrodynamical equations with gravity for modelling the nonstationary processes in rotating gaseous bodies are:

$$\frac{d\mathbf{x}}{dt} = \mathbf{v}, \quad \frac{d\rho}{dt} + \rho \nabla \cdot \mathbf{v} = 0, \quad \rho \frac{d\mathbf{v}}{dt} = -\nabla(P) - \rho \nabla \Phi, \quad (2)$$

$$\rho \frac{d\varepsilon}{dt} + P \nabla \cdot \mathbf{v} + \rho F(\rho, T) = 0, \quad \Delta \Phi = 4\pi G \rho.$$

Here the equation of state and the function of neutrino losses have been represented by following functions

$$P \equiv P(\rho, T) = P_0(\rho) + \rho \mathfrak{R}T + \frac{\sigma T^4}{3}, \quad \varepsilon = \varepsilon_0(\rho) + \frac{3}{2} \mathfrak{R}T + \frac{\sigma T^4}{\rho} + \varepsilon_{Fe}(\rho, T), \quad (3)$$

where $\varepsilon_{Fe}(\rho, T)$ is the iron dissociation energy, $F(\rho, T)$ is the function of neutrino losses, among which only the URCA process losses are important. Other losses, such as pair annihilation, photo production of neutrino, plasma neutrino were also included in the calculations.

$$P_0(\rho) = \begin{cases} P_0^{(1)} & = b_1 \rho^{1/3} / (1 + c_1 \rho^{1/3}), & \rho \leq \rho_1, \\ P_0^{(k)} & = a \cdot 10^{b_k (\lg \rho - 8.419)^{c_k}} & \rho_{k-1} \leq \rho \leq \rho_k, \quad k = \overline{2, 6} \end{cases} \quad (4)$$

$$\varepsilon = \varepsilon_0(\rho) + \frac{3}{2} \mathfrak{R}T + \frac{\sigma T^4}{\rho} + \varepsilon_{Fe}(\rho, T), \quad \varepsilon_0(\rho) = \int_0^{\rho} \frac{P_0(\tilde{\rho})}{\tilde{\rho}^2} d\tilde{\rho}, \quad \varepsilon_{Fe}(\rho, T) = \frac{E_{b,Fe}}{A m_p} \left(\frac{T - T_{0Fe}}{T_{1Fe} - T_{0Fe}} \right). \quad (5)$$

$$f(\rho, T) = \frac{1.3 \cdot 10^9 \mathfrak{a}(\overline{T}) \overline{T}^6}{1 + (7.1 \cdot 10^{-5} \rho / \overline{T}^3)^{2/5}} \text{ erg} \cdot \text{g}^{-1} \cdot \text{s}^{-1}, \quad \overline{T} = T \cdot 10^{-9}, \quad (6)$$

$$\mathfrak{a}(T) = \begin{cases} 1, & \overline{T} < 7, \\ 664.31 + 51.024(\overline{T} - 20), & 7 \leq \overline{T} \leq 20, \\ 664.31, & \overline{T} > 20, \end{cases} \quad (7)$$

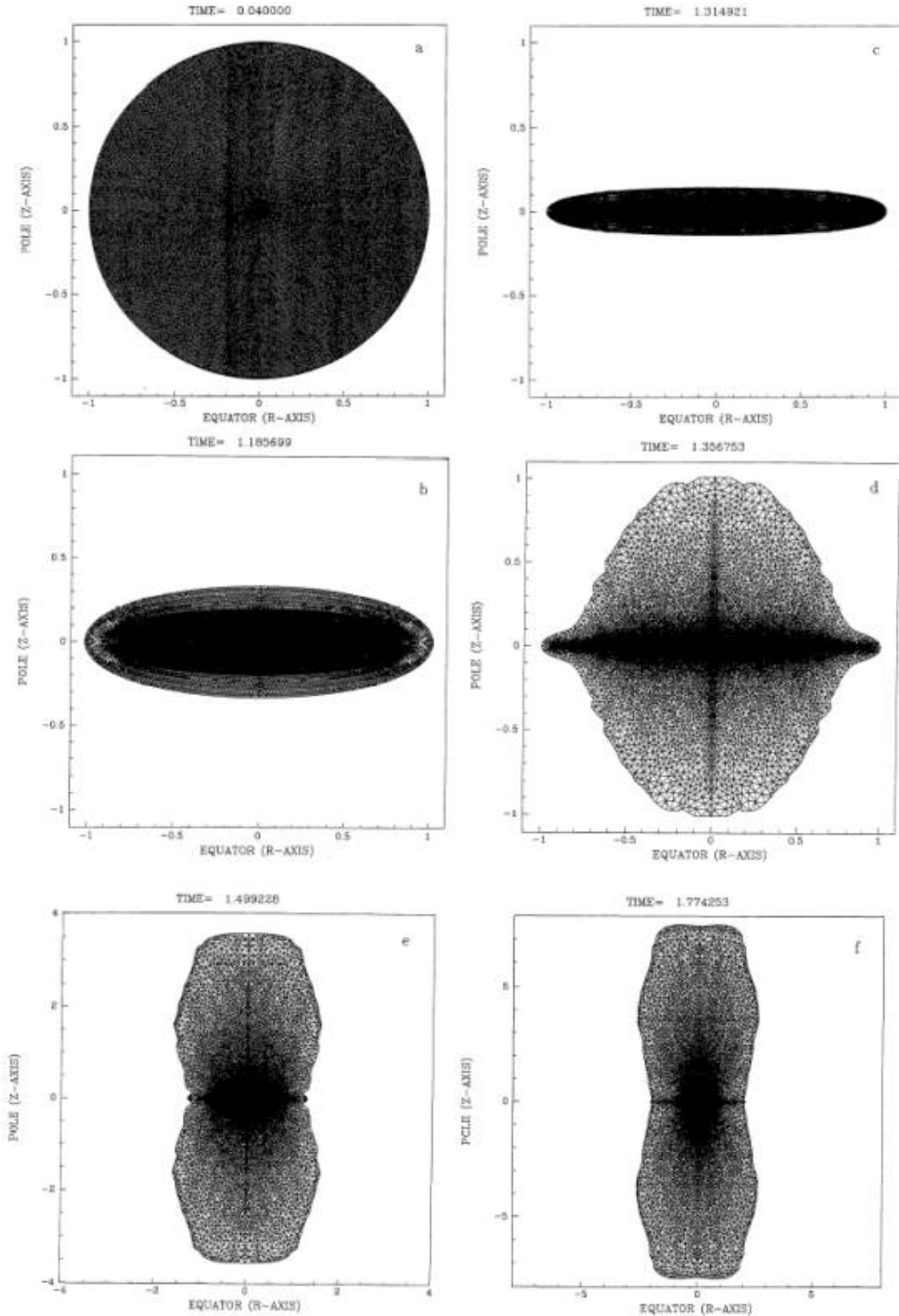


Figure 10: Time evolution of the shape of the rotating collapsing gas cloud, from [1].

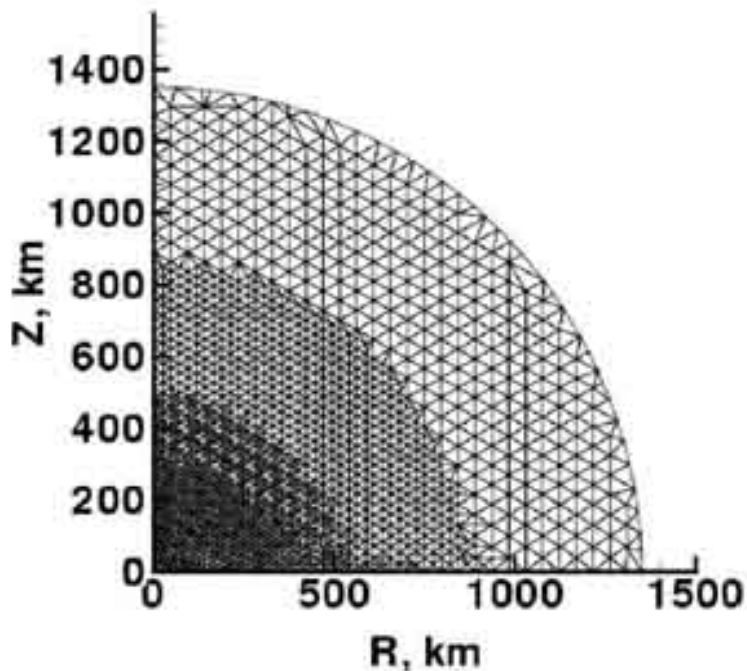


Figure 11: The triangle grid at the beginning, $t = 0$, from [2].

The URCA losses $f(\rho, T)$ have been described by formula [12], obtained by approximation of tables from [17]. Other losses (unimportant) are included in Q_{tot} .

$$F(\rho, T) = (f(\rho, T) + Q_{tot})e^{-\frac{\tau_\nu}{10}}. \quad (8)$$

Neutrino absorption is important in deeper layers of the neutron star. It is taken into account implicitly, by multiplying the transparent neutrino flux by the multiplier $e^{-\frac{\tau_\nu}{10}}$, where the effective neutrino optical depth τ_ν is calculated using local density gradients [2],[4]. Initial state was chosen as a spherically symmetric star, with a mass 20% larger than the limiting mass of the corresponding white dwarf $M = 1,0042M_\odot + 20\%$, and rotating uniformly, with an angular velocity 2.519 (1/sec). The temperature distribution was taken in the form $T = \delta\rho^{2/3}$. The initial triangular grid covering a quarter of the circle, where equations are solved, is represented in Fig.11.

Results of calculations are represented in Figs.12 - 14. The collapse is stopped due to formation of a stable neutron core, rotating almost uniformly. The shock is reflected from the core, leaving behind a hot plasma, where vortexes are generated. It leads to a strong mixing, what is important for the interpretation of observations of the light curve of SN 1987A. The light curve, corresponding to the radioactive decay of $^{56}\text{Ni} \rightarrow ^{56}\text{Co} \rightarrow ^{56}\text{Fe}$ was observed in this object, what could be explained by enrichment of the outbursting matter due to mixing with deeper layers.

The main result of these calculations is a self-consistent model of the rapidly rotating neutron star with a differentially rotating envelope. The adjusting parameters are chosen to reproduce the calculations with a refined account of the neutrino transport [13]. In correspondence with these calculations we have obtained that the bounce shock wave and neutrino deposition do not produce SN explosion. Distribution of the angular velocity is represented in Fig.14. The period of rotation of the almost uniformly rotating core of the young neutron star is about 0.001 sec.

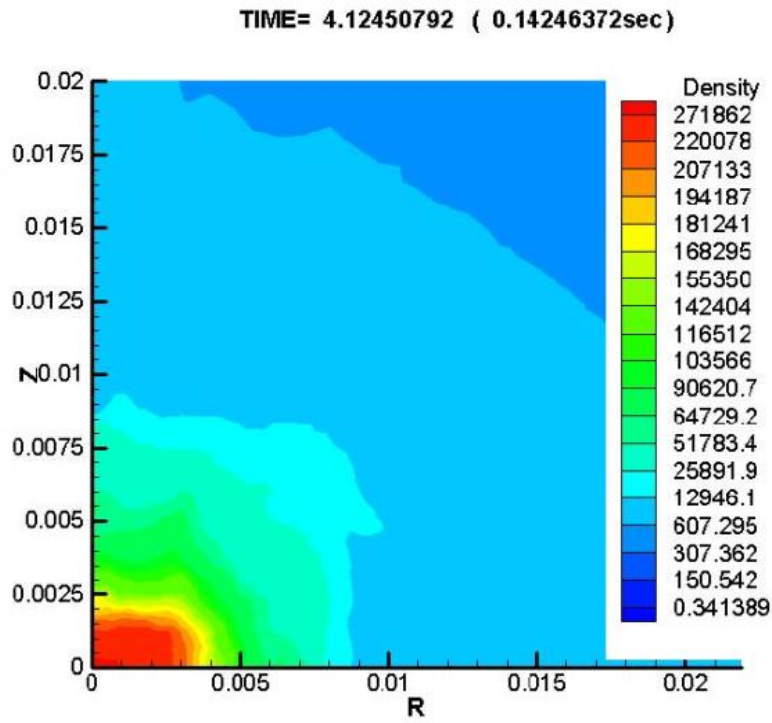


Figure 12: Density distribution in the central region at maximum compression state $t = 0.1425$ sec, from [2].

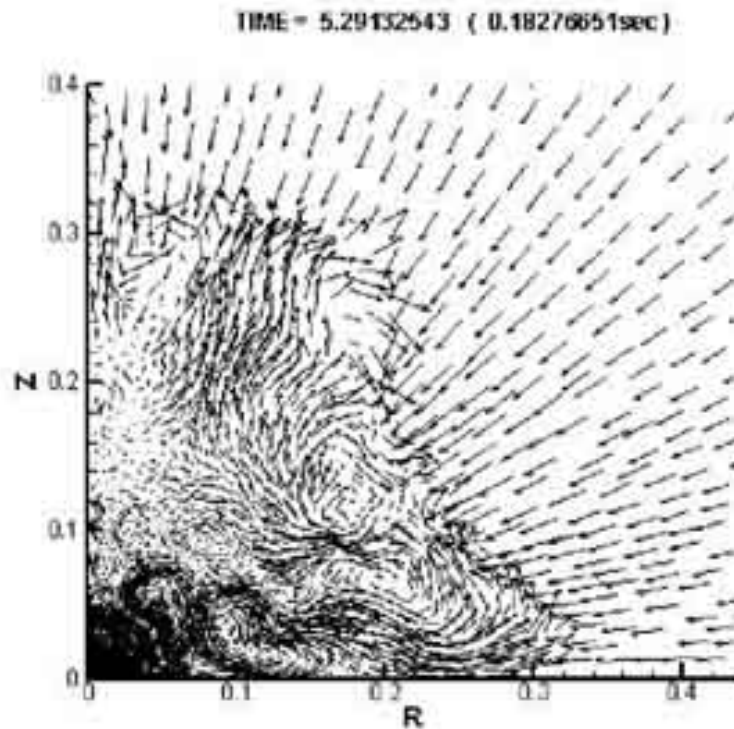


Figure 13: Velocity field, showing mixing of matter behind the shock at $t = 0.1828$, from [2].

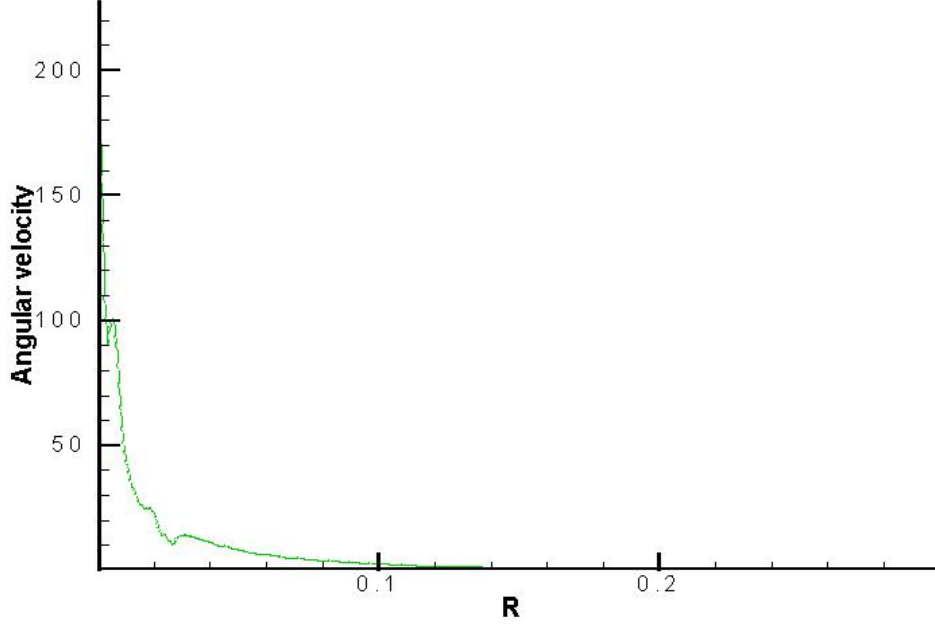


Figure 14: Angular velocity distribution in the equatorial plane of the new born neutron star at $t = 0.261$ after the beginning of the collapse.

5 2-D magnetorotational supernova

Calculations of magnetorotational core-collapse supernova have been performed in [4]. Magnetohydrodynamic (MHD) equations with self-gravitation, and infinite conductivity have been solved using the same numerical scheme as described above. The set of equations is the following:

$$\begin{aligned} \frac{d\mathbf{x}}{dt} = \mathbf{v}, \quad \frac{d\rho}{dt} + \rho\nabla \cdot \mathbf{v} = 0, \quad \rho \frac{d\mathbf{v}}{dt} = -\text{grad} \left(P + \frac{\mathbf{H} \cdot \mathbf{H}}{8\pi} \right) + \frac{\nabla \cdot (\mathbf{H} \otimes \mathbf{H})}{4\pi} - \rho\nabla\Phi, \\ \rho \frac{d}{dt} \left(\frac{\mathbf{H}}{\rho} \right) = \mathbf{H} \cdot \nabla \mathbf{v}, \quad \Delta\Phi = 4\pi G\rho, \quad \rho \frac{d\varepsilon}{dt} + P\nabla \cdot \mathbf{v} + \rho F(\rho, T) = 0, \quad P = P(\rho, T), \quad \varepsilon = \varepsilon(\rho, T), \end{aligned} \quad (9)$$

where $\frac{d}{dt} = \frac{\partial}{\partial t} + \mathbf{v} \cdot \nabla$ is the total time derivative, $\mathbf{x} = (r, \varphi, z)$, $\mathbf{v} = (v_r, v_\varphi, v_z)$ is the velocity vector, ρ is the density, P is the pressure, $\mathbf{H} = (H_r, H_\varphi, H_z)$ is the magnetic field vector, Φ is the gravitational potential, ε is the internal energy, G is gravitational constant, $\mathbf{H} \otimes \mathbf{H}$ is the tensor of rank 2, and $F(\rho, T)$ is the rate of neutrino losses. Equation of state and the function of neutrino losses have been the same as in the previous section. Additional condition here is $\text{div}\mathbf{H} = 0$. The problem has an axial symmetry ($\frac{\partial}{\partial \varphi} = 0$), and the symmetry to the equatorial plane ($z=0$). Boundary conditions are the following:

$$P = \rho = T = B_\phi = 0 \text{ at the outer boundary; } \quad v_r = j_r = B_r = 0 \text{ at } r = 0; \quad (10)$$

$$v_\phi = j_\phi = B_\phi = 0 \text{ at } r = 0; \quad v_z = 0, \quad \frac{\partial B_z}{\partial z} = 0 \text{ (dipole-like) or } B_z = 0 \text{ (quadrupole-like) at } z = 0.$$

Initial toroidal current J_ϕ (see Fig.15) was taken at the initial moment (time started now from the stationary rotating neutron star) producing H_r, H_z according to Bio-Savara law

$$\mathbf{H} = \frac{1}{c} \int_V \frac{\mathbf{J} \times \mathbf{R}}{R^3} dV, \quad (11)$$

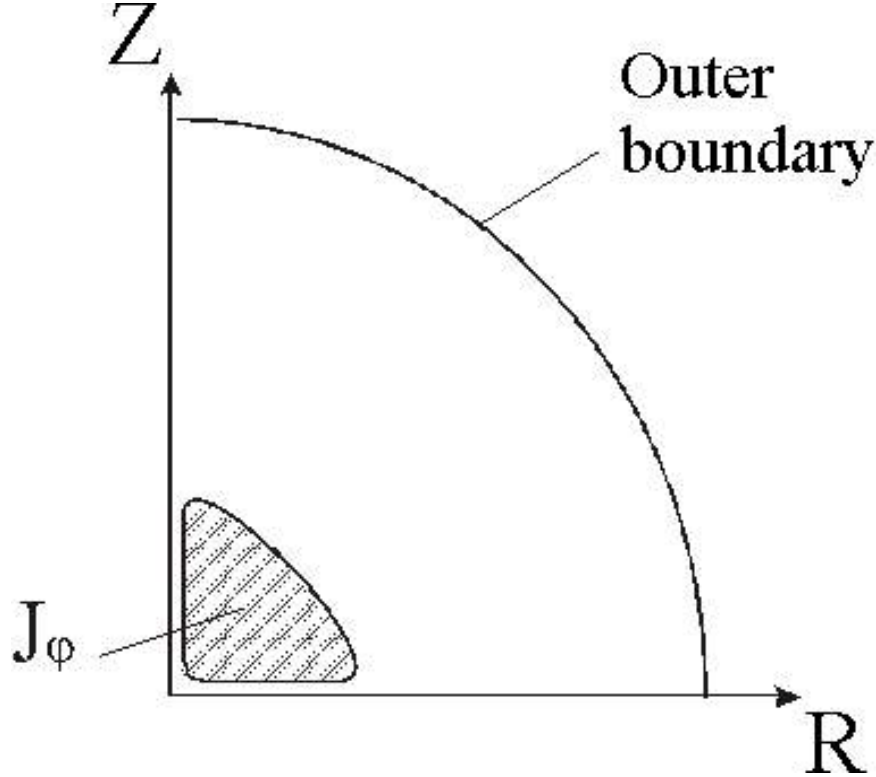


Figure 15: Initial, at $t = 0$, current distribution in the upper hemisphere. Dipole-like field is obtained when currents in both hemispheres have the same sign, and quadrupole-like field appears when currents have opposite signs.

Initial magnetic field of quadrupole-like symmetry is obtained by opposite directions of the current in both hemispheres (Fig.16). Magnetic field is amplified due to twisting by the differential rotation, and subsequent development of the magnetorotational instability. The field distribution for initial quadrupole-like magnetic field with $\alpha = 10^{-6}$, at the moment of the maximal energy of the toroidal magnetic field is represented in Fig.17. Two dark areas: near the equatorial plane, and around the axis at 45° , show the regions with local maxima of the toroidal magnetic field H_ϕ^2 . The maximal value of $H_\phi = 2.5 \cdot 10^{16}$ Gs was obtained in the calculations. The magnetic field at the surface of the neutron star after the explosion is $H = 4 \cdot 10^{12}$ Gs. Temperature and velocity fields development with time is given in Fig.18. Time dependencies during the explosion of different types of the energy: rotational energy, gravitational energy, internal energy, kinetic poloidal energy, are given in Figs.19. The evolution of the magnetic poloidal energy and magnetic toroidal energies are given in the right side of Fig.20. Distribution of the specific angular momentum rv_ϕ at different time moments is given in Fig.20 (left), and Fig.21.

Almost all gravitational energy, transforming into heat during the collapse, is carried away by weakly interacting neutrino. Dependence of the neutrino luminosity, and integral neutrino losses on time are represented in Fig.22. A mass "particle" is considered ejected if its kinetic energy is greater than its potential energy. Time dependence of the ejected mass in (M_\odot), and the ejected energy during the magnetorotational explosion with a quadrupole-like field are represented in Fig.23. The total energy ejected in the kinetic form is equal to $0.6 \cdot 10^{51}$ erg, and the total ejected mass is equal to $0.14M_\odot$.

6 Magnetorotational instability

Magnetorotational instability (MRI) leads to exponential growth of magnetic fields. Different types of MRI have been studied in [15],[22],[8],[21]. MRI starts to develop when the ratio of the toroidal to the poloidal magnetic energies is becoming large. In 1-D calculations MRI is absent because of a

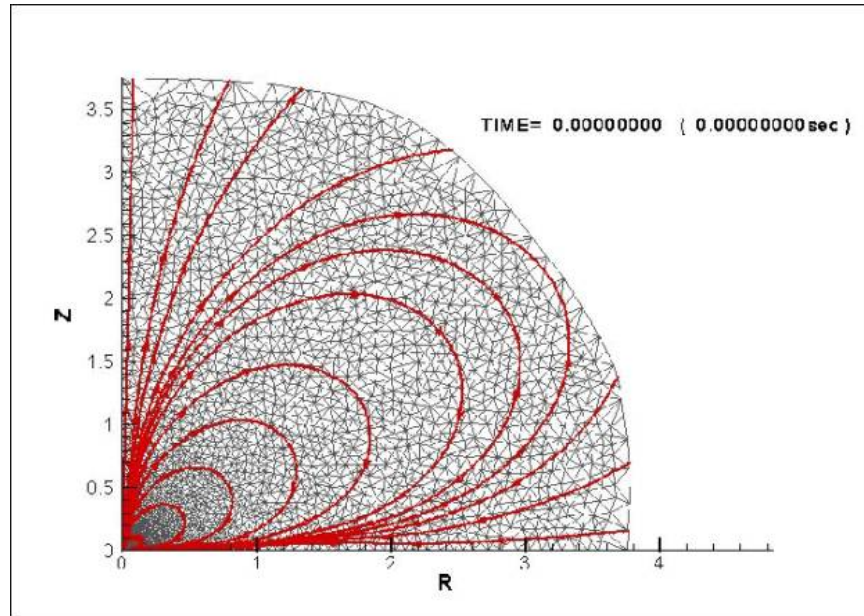


Figure 16: Initial quadrupole-like magnetic field, at $t = 0$.

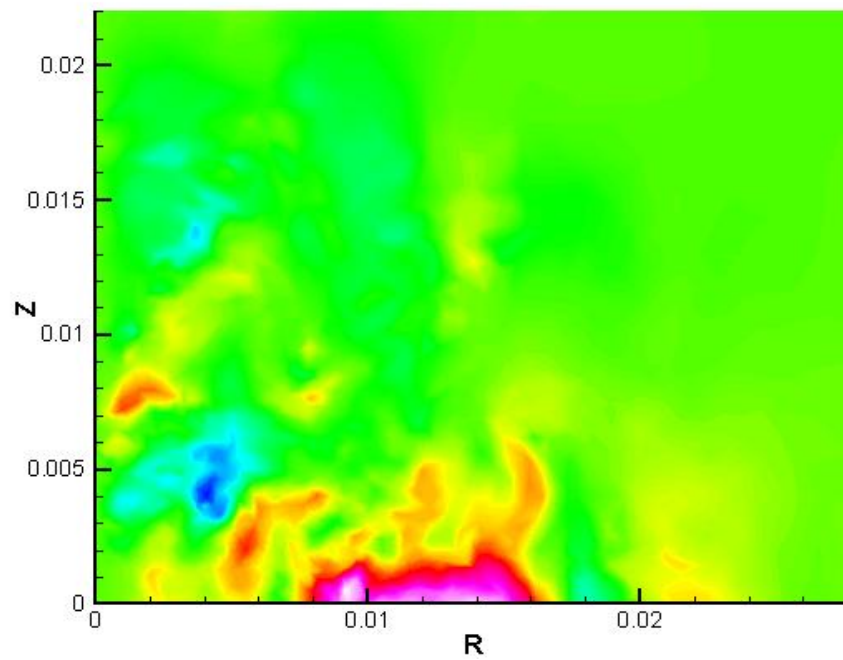


Figure 17: Toroidal magnetic field distribution at the moment of its maximal energy.

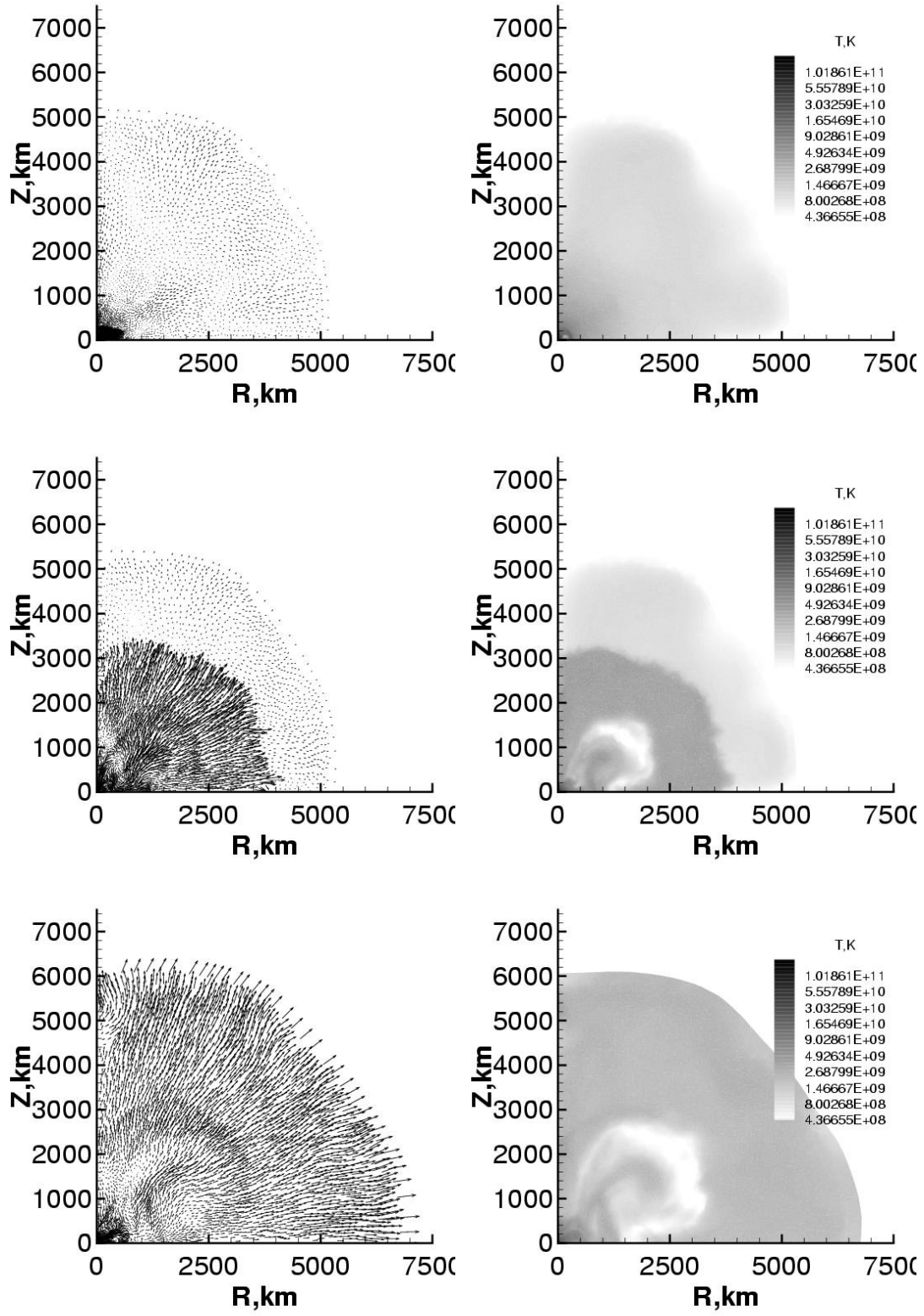


Figure 18: Time evolution of the velocity field (left column) and temperature (right column) for the time moments $t = 0.07s$, $0.20s$, $0.30s$, from [4].

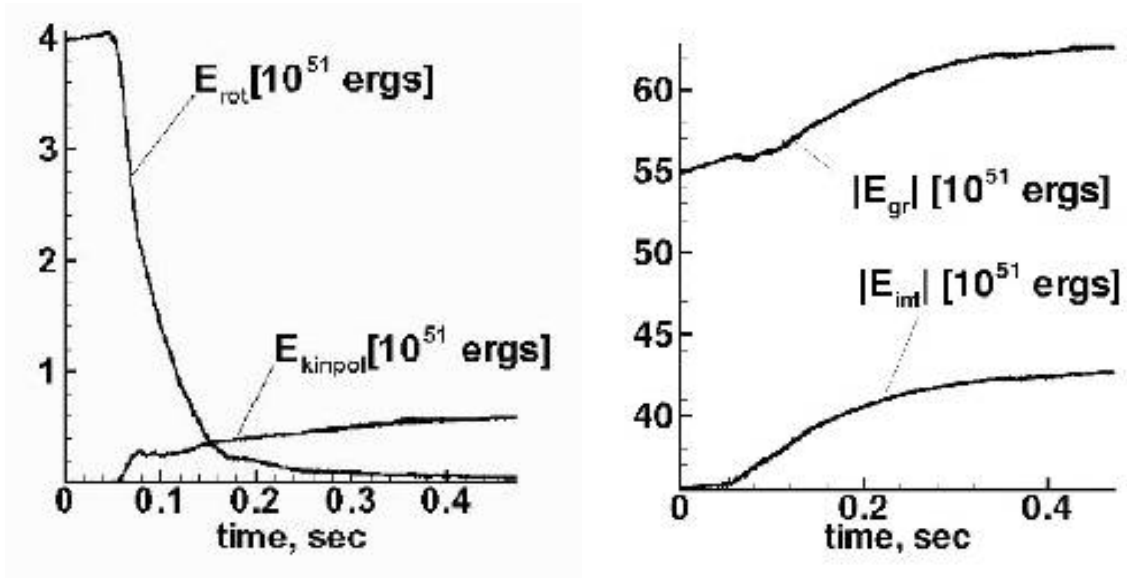


Figure 19: Time dependence of the gravitational, internal, rotational, and kinetic poloidal energies of the star during magnetorotational explosion with a quadrupole-like field, from [4].

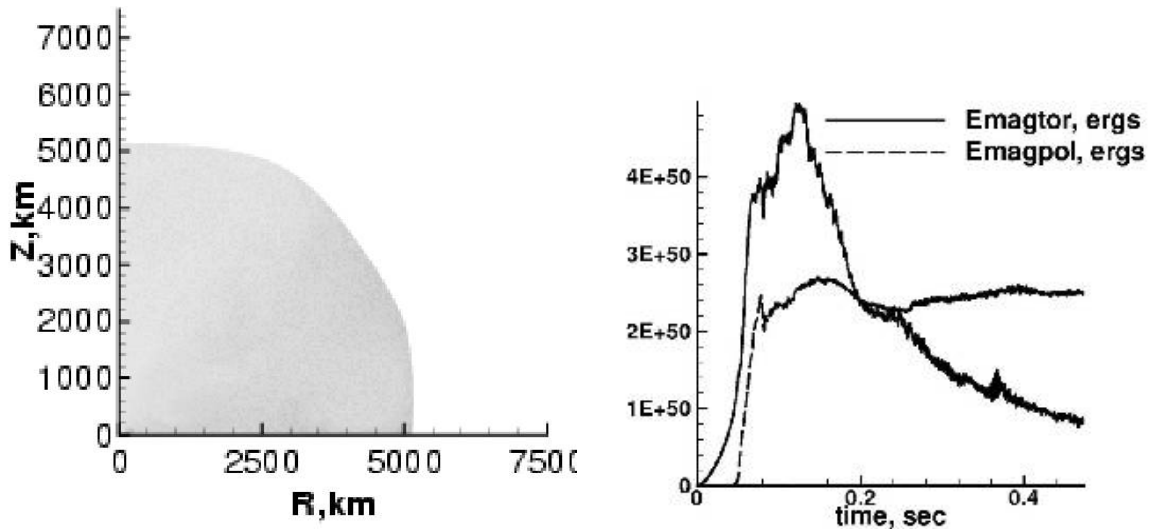


Figure 20: **Right** Time dependencies of the magnetic (toroidal and poloidal separately) energies of the star during magnetorotational explosion with a quadrupole-like field. **Left** The specific angular momentum $v_\phi r$ distribution for the time moment $t = 0.07s$, from [4]

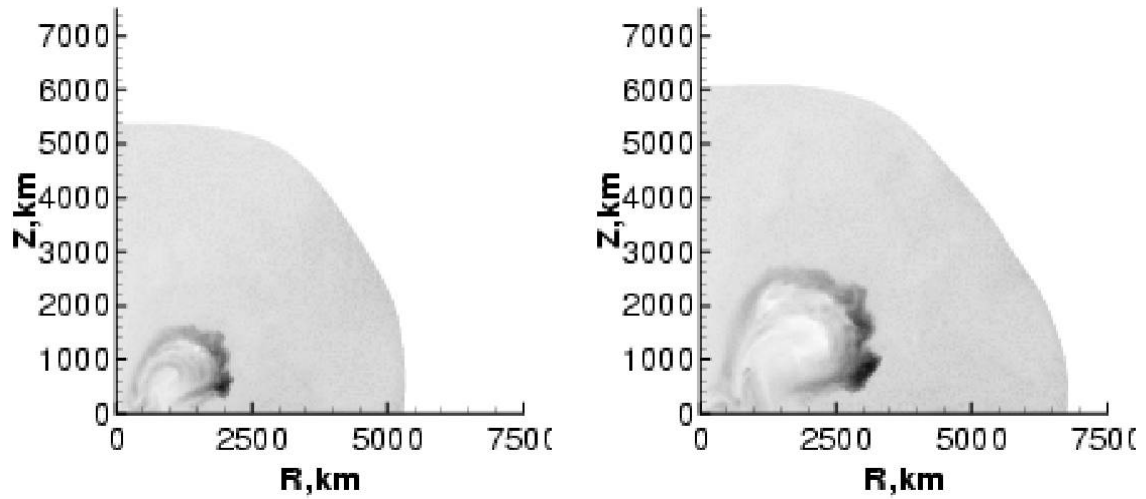


Figure 21: Time evolution of the specific angular momentum $v_{\phi}r$ for the time moments $t = 0.20s, 0.30s$. The darker parts of the plots correspond to the higher specific angular momentum, from [4].

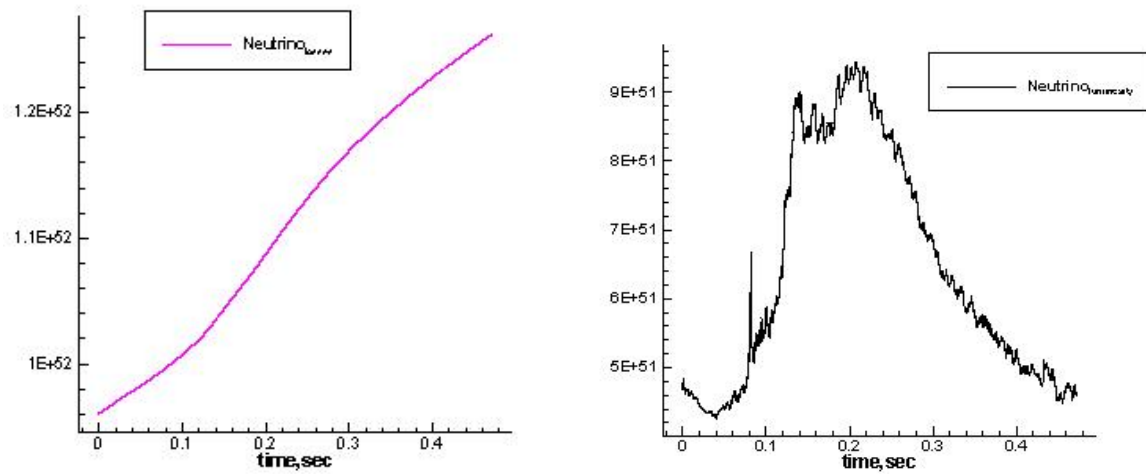


Figure 22: The integral neutrino losses (**right**), and neutrino luminosity $\int_0^{M_{core}} f(\rho, T) dm$ (**left**), as a function of time during the magnetorotational explosion, from [4].

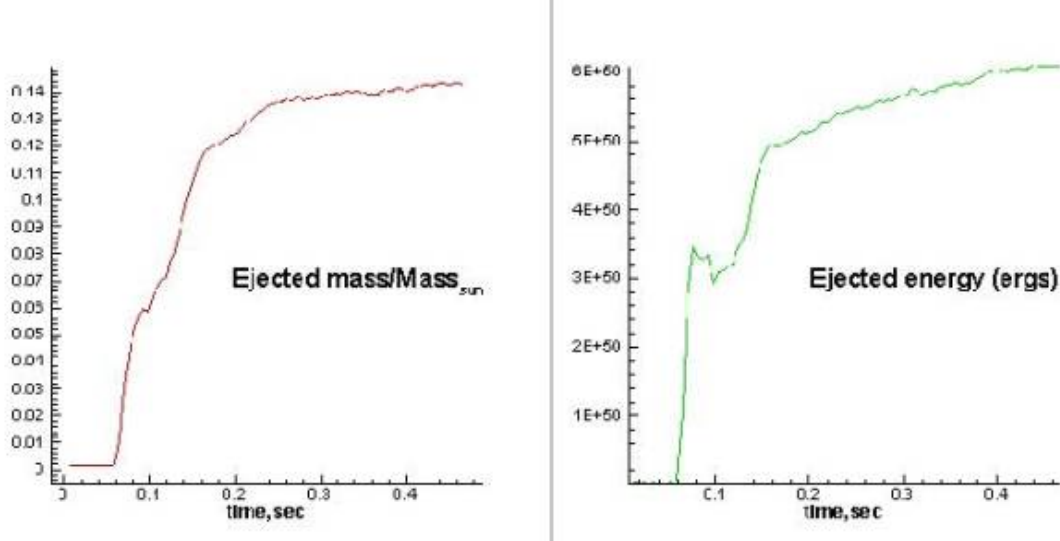


Figure 23: Time dependence of the ejected mass in (M_{\odot}), and ejected energy during the magnetorotational explosion with a quadrupole-like field. The particle is considered as ejected if its kinetic energy is greater than its potential energy and its velocity vector is directed from the center, from [4].

restricted degree of freedom. Therefore the time of the MR explosion is increasing with α as $t_{\text{expl}} \sim \frac{1}{\sqrt{\alpha}}$, $\alpha = \frac{E_{\text{mag}0}}{E_{\text{grav}0}}$. Due to the development of MRI the time of the MR explosion depends on α much weaker. The ratio of two magnetic energies is changing with time almost with the same speed for all α , so MRI starts almost at the same time. The MR explosion happens when the magnetic energy is becoming comparable to the internal energy, at least in some parts of the star. While the starting magnetic energy linearly depends on α , and MRI leads to exponential growth of the magnetic energy, the total time of MRE in 2-D is growing **logarithmically** with decreasing of α , $t_{\text{expl}} \sim -\log \alpha$. These dependencies are seen clearly from 1-D and 2-D calculations with different α giving the following explosion times t_{expl} (in arbitrary units):

$$\begin{aligned} \alpha = 0.01, t_{\text{expl}} = 10, \quad \alpha = 10^{-12}, t_{\text{expl}} = 10^6 \quad & \text{in 1-D} \\ \alpha = 10^{-6}, t_{\text{expl}} \sim 6, \quad \alpha = 10^{-12}, t_{\text{expl}} \sim 12 \quad & \text{in 2-D} \end{aligned} \quad (12)$$

6.1 Toy model of the MRI development

Toy model of the MRI development shows an exponential growth of the magnetic fields at initial stages of MRI development in 2-D. Initially MRI leads to formation of multiple poloidal differentially rotating vortices. Angular velocity of vortices is growing (linearly) with a growth of H_{φ} .

$$\frac{dH_{\varphi}}{dt} = H_r \left(r \frac{d\Omega}{dr} \right). \quad (13)$$

The right-hand side is constant at the initial stage of the process. When the toroidal field reaches its critical value H_{φ}^* , the MRI instability starts to develop. As follows from our calculations, the critical value corresponds to the ratio between total over the star toroidal and poloidal magnetic energies $\sim 1 - 3$. A local value of this critical ratio is much larger, reaching at the beginning of MRI $\sim 10^4$ in the regions of the maximal growth of the toroidal magnetic field, what in time roughly corresponds to about 100 rotations of the neutron star core. These regions serve as germs for subsequent development of MRI in other parts of the star. The appearance of MRI is characterized by formation of multiple *poloidal* differentially rotating vortices, which twist the initial poloidal field leading to its amplification

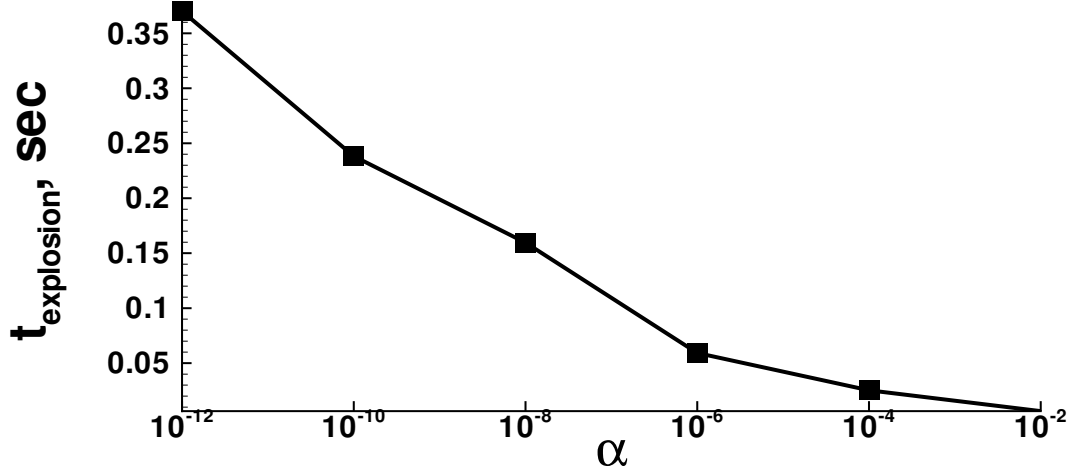


Figure 24: Duration of the explosion time on α in presence of MRI, from [19]

according to

$$\frac{dH_r}{dt} = H_{r0} \left(\frac{d\omega_v}{dl} l \right), \quad (14)$$

where l is the coordinate, directed along the vortex radius, ω_v is the angular velocity of the poloidal vortex. Qualitatively the poloidal field amplification due to the vortices induced by MRI is shown in the Fig. 25. The enhanced poloidal field immediately starts to take part in the toroidal field amplification according to (13). With further growing of H_φ the poloidal vortex speed increases. Our calculations give the values of $\omega_v = 0.0132 \text{ s}^{-1}$ at $|H_\varphi| = 2.46 \cdot 10^{15} \text{ G}$ corresponding to $t = 0.041 \text{ s}$ and $\omega_v = 0.052 \text{ s}^{-1}$ at $|H_\varphi| = 4.25 \cdot 10^{15} \text{ G}$ corresponding to $t = 0.052 \text{ s}^{-1}$ for the same Lagrangian particle. In general we may approximate the value in brackets (14) by linear function on the value $(H_\varphi - H_\varphi^*)$ as

$$\left(\frac{d\omega_v}{dl} l \right) = \alpha (H_\varphi - H_\varphi^*). \quad (15)$$

$$\frac{d^2}{dt^2} (H_\varphi - H_\varphi^*) = A H_{r0} \alpha (H_\varphi - H_\varphi^*), \quad (16)$$

$$H_\varphi = H_\varphi^* + H_{r0} e^{\sqrt{A\alpha H_{r0}}(t-t^*)},$$

$$H_r = H_{r0} + \frac{H_{r0}^{3/2} \alpha^{1/2}}{\sqrt{A}} \left(e^{\sqrt{A\alpha H_{r0}}(t-t^*)} - 1 \right),$$

7 Jet formation in MRE

Jet formation in MRE happens when the initial magnetic field is of a dipole-like structure. 2-D calculations with the initial dipole-like magnetic field gave almost the same values of the energy of explosion $\sim 0.5 \cdot 10^{51} \text{ erg}$, and ejected mass $\approx 0.14 M_\odot$ (see Figs.26), but the outburst was slightly collimated along the rotational axis [19].

7.1 Violation of mirror symmetry of magnetic field

There is a violation of the mirror symmetry of magnetic field when two components dipole + quadrupole are present from the beginning [23]. Another possibility of violation of the mirror symmetry of magnetic

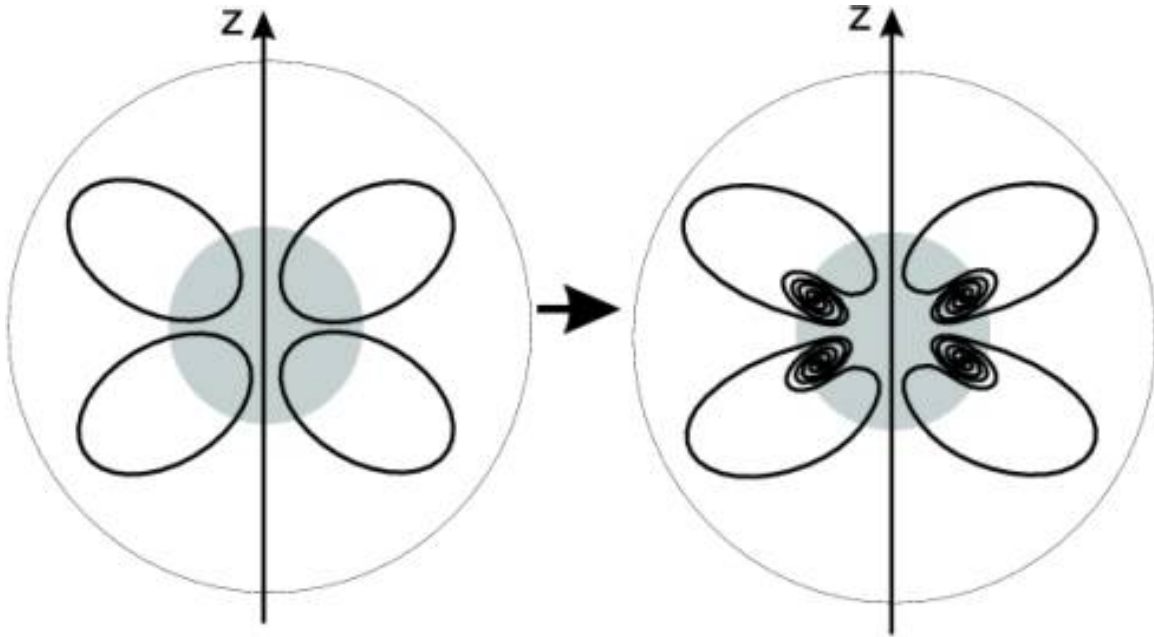


Figure 25: Qualitative picture of the development of the MRI in 2-D.

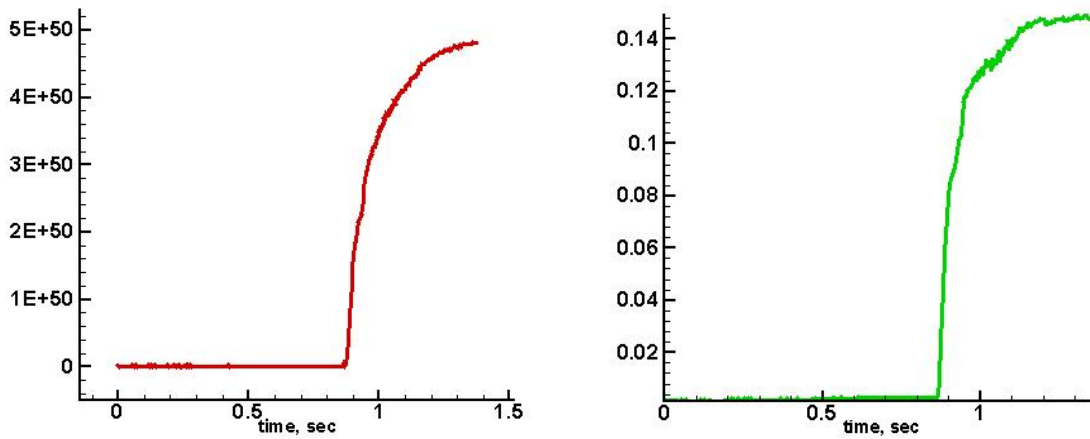


Figure 26: **(Left)** Time dependence of the ejected energy during the magnetorotational explosion with a dipole-like field. **(right)** Time dependence of the ejected mass during the magnetorotational explosion with a dipole-like field, from [19].

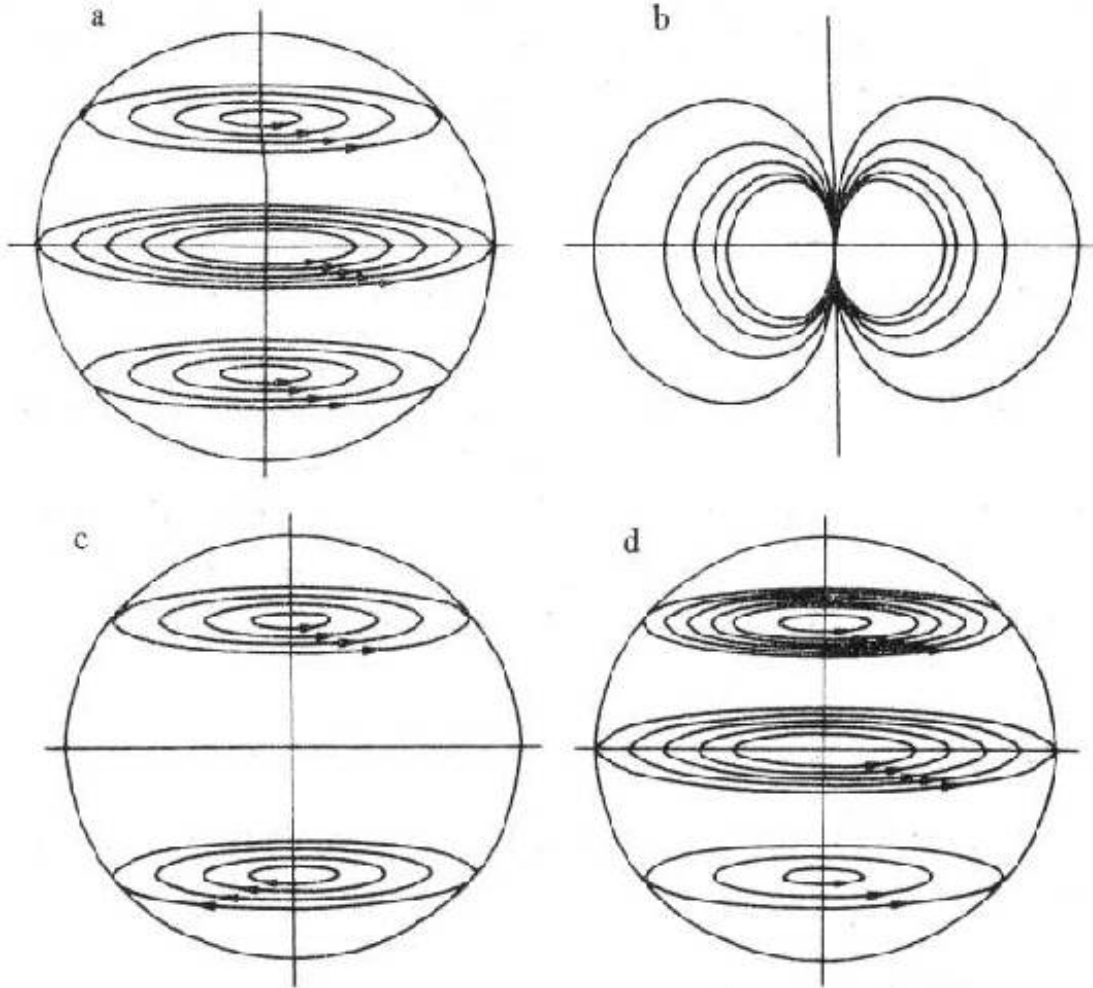


Figure 27: Loss of a mirror symmetry of the magnetic field in the differentially rotating star, from [11].

field was considered in [11]. If we start from axially symmetric configuration with a mixture of poloidal and toroidal fields with different parity, than any exchange between these two components will lead to such violation. For example, if we start from the dipole-like poloidal field (negative parity), and symmetric toroidal field with a positive parity, than twisting of the dipole magnetic field by the differential rotation leads to creation of additional toroidal field with a negative parity, Therefore the total resulting toroidal field will become asymmetric relative to the equatorial plane, see Fig.27.

The magnetorotational explosion with a mirror asymmetric field will be always asymmetrical. A kick velocity due to such asymmetry of the magnetic field could be up to ~ 300 km/sec [11]. The interaction of the neutrino with asymmetric magnetic field could increase the kick velocity up to ~ 1000 km/sec, giving a possibility to explain the origin of velocities of the most rapidly moving pulsars [10].

8 Conclusions

1. In the magnetorotational explosion (MRE) the efficiency of transformation of rotational energy into the energy of explosion is 10%. This is enough for producing core collapse SN from rapidly rotating magnetized neutron star.

2. Development of magneto-rotational instability strongly accelerates MRE, at lower values of the initial magnetic fields.

3. The new born neutron star has inside a large (about 10^{14} Gauss) chaotic magnetic field.
4. Jet formation is possible for dipole-like initial topology of the field, what may have a possible relation to cosmic gamma-ray bursts; equatorial ejection happens at prevailing of the quadrupole-like component.
5. Braking of the equatorial symmetry happens in differentially rotating star with toroidal and poloidal components of an opposite symmetry; it may explain formation of the rapidly moving pulsars and one-side jet formation.

Acknowledgement. G.S.B.-K. is grateful to the organizers of the conference for support and hospitality. G.S.B.-K. and S.G.M. Thanks RFBF for the partial support in the frame of the grant 05-02-17697.

References

- [1] Ardeljan, N.V., Bisnovatyi-Kogan, G.S., Kosmachevskii, K.V., Moiseenko, S.G. (1996) An implicit Lagrangian code for the treatment of nonstationary problems in rotating astrophysical bodies. *Astron. Ap. Suppl.* **115** 573-594.
- [2] Ardeljan, N.V., Bisnovatyi-Kogan, G.S., Kosmachevskii, K.V., Moiseenko, S.G. (2004) Two-Dimensional Simulation of the Dynamics of the Collapse of a Rotating Core with Formation of a Neutron Star on an Adaptive Triangular Grid in Lagrangian Coordinates. *Astrophysics* **47** 37-51.
- [3] Ardeljan, N.V., Bisnovatyi-Kogan, G.S., Moiseenko, S.G. (2000) Nonstationary magnetorotational processes in a rotating magnetized cloud. *Astron. Ap.* **355** 1181-1190.
- [4] Ardeljan, N. V., Bisnovatyi-Kogan, G. S., Moiseenko, S. G. (2005) Magnetorotational supernovae. *Month. Not. Roy. Astron. Soc.* **359** 333-344.
- [5] Ardeljan, N.V., Bisnovatyi-Kogan, G.S., Popov, Yu.P. (1979) The investigation of a magnetorotational explosion of a supernova in a cylindrical model. *Astron. Zh.* **56**, 1244-1255 (*Soviet Astronomy* **23** 705-711).
- [6] Ardeljan, N.V., Bisnovatyi-Kogan, G.S., Popov, Yu.P., Chernigovsky, S.V. (1987) Core Collapse and Formation of a Rapidly Rotating Neutron Star. *Astron. Zh.* **64** 761-772 (*Soviet Astronomy* **31**, 398-403).
- [7] Ardeljan, N.V, Kosmachevskii, K.V. (1995) Implicit free-lagrange method for computing two-dimencional magnetogas-dynamic flows. *Computational mathematics and modeling* **6** 209-224.
- [8] Balbus, S.A., Hawley, J.F. (1998) Instability, turbulence, and enhanced transport in accretion disks. *Rev. Mod. Phys.* **70** 1-53.
- [9] Bisnovatyi-Kogan, G.S. (1970) The Explosion of a Rotating Star As a Supernova Mechanism. *Astron. Zh.* **47** 813-816 (*Soviet Astronomy* (1971) **14** 652-655).
- [10] Bisnovatyi-Kogan, G.S. (1993) Asymmetric neutrino emission and formation of rapidly moving pulsars. *Astron. Ap. Transactions* **3** 287-294.
- [11] Bisnovatyi-Kogan, G.S., Moiseenko, S.G. (1992) Violation of Mirror Symmetry of the Magnetic Field in a Rotating Star and Possible Astrophysical Manifestations. *Soviet Astr.* **36** 285-288.
- [12] Bisnovatyi-Kogan, G.S., Popov, Yu.P., Samokhin, A.A. (1976) The magnetohydrodynamic rotational model of supernova explosion. *Ap. Space Sci.* **41** 287-320.
- [13] Buras, R., Rampp, M., Janka, H.-Th., Kifonidis, K. (2003) mproved Models of Stellar Core Collapse and Still No Explosions: What Is Missing? *Physical Review Letters* **90** 241101(1-4).
- [14] Chandrasekhar S. (1981) *Hydrodynamic and Hydromagnetic stability*. New York, Dover.
- [15] Dungey J.W. (1958) *Cosmic electrodynamics*. Cambridge Univ. Press, Cambridge.
- [16] Iben, I., Jr. (1985) The life and times of an intermediate mass star - In isolation/in a close binary. *Quarterly Journal Royal Astron. Soc.* **26** 1-39.
- [17] Ivanova L.N., Imshennik V.S., Nadezhin D.K. (1969) *Nauchn. Inform. Astron. Sov. Akad. Nauk SSSR (Sci. Inf. of the Astr. Council of the Acad. Sci. USSR)* **13** 3-96.

- [18] Leblanc, L.M., Wilson, J.R. (1970) A Numerical Example of the Collapse of a Rotating Magnetized Star. *ApJ* **161** 541-551.
- [19] Moiseenko, S.G., Bisnovaty-Kogan, G.S., Ardeljan, N.V. (2005) Magnetorotational supernovae - the supernova mechanism that works. *Memorie della Societa Astronomica Italiana*, **76**, 575-579.
- [20] Pols, O.R., Tout, C.A., Eggleton, P.P., Han, Z. (1995) Approximate input physics for stellar modelling. *Mon.Not.Roy.Astron.Soc.* **274** 964-974.
- [21] Spruit, H.C. (2002) Dynamo action by differential rotation in a stably stratified stellar interior. *Astron. Ap.* **381** 923-932.
- [22] Velikhov E.P., (1959), Stability of an ideally conducting liquid flowing between rotating cylinders in a magnetic field. *J. Exper. Theor. Phys.* **36** 1398-1404.
- [23] Wang, J.C.L., Sulkanen, M.E., Lovelace, R.V.E. (1992) Intrinsically asymmetric astrophysical jets. *Astrophys. J.* **390** 46-65.